THE ANNALS OF "DUNAREA DE JOS" UNIVERSITY OF GALATI
FASCICLE XIV MECHANICAL ENGINEERING, ISNN1224-5615
2006

EVALUATION OF THERMAL STRESSES IN THERMO-ABRASIVE BLASTING NOZZLES

Prof. dr. ing. Igor A. Gorlach
Nelson Mandela Metropolitan University,
South Africa

ABSTRACT

Thermo-abrasive blasting is a technique, which combines conventional abrasive blasting and HVAF processes to prepare surfaces prior coating. Thermo-abrasive blasting has a number of advantages over conventional abrasive blasting as the result of a higher nozzle pressure and heat, which helps to remove impurities from the surface. However, practice showed that the short life of blasting nozzles due to thermal stresses and excessive wear is the biggest drawback of this method. Therefore, the correct nozzle geometry and suitable materials are critical for an efficient operation of thermo-abrasive blasting systems. In this study, computational fluid dynamics and finite element analyses were used to obtain the temperature distribution and to evaluate thermal stresses in nozzle materials. The materials investigated include tungsten carbide-cobalt (WC-6wt.% Co), hot pressed dense silicon carbide (SiC) and SiALON (Si_3N_4-Al_2O_3-AlN). The analysis and experiments showed that WC-CO nozzles produce the best overall results of thermal shock resistance and wear in thermo-abrasive blasting.

1. Introduction

Conventional abrasive blasting nozzles are subjected mainly to wear. Thermo-abrasive blasting nozzles, besides wear, must also withstand high temperatures. The most common abrasive blasting nozzle material is WC-Co of different grades. Ceramics, such as boron carbide, silicon carbide and SiALON, are less common, but with advances in material science, there is an increase in ceramic applications for abrasive blasting.

Since HVAF and HVOF systems were introduced in coating processes, there was a need for nozzles which could be wear resistant and withstand high temperatures. There have been attempts to use various ceramics for spray nozzles, for example, a nozzle constructed by machining a graphite tube, and then coating the graphite tube with silicon carbide was suggested [1]. In another example, nozzle inserts made of a solid dense silicon carbide were reported [2]. Thermal shock still poses a problem to ceramic nozzles and sudden start-ups or shut-downs can cause a nozzle to crack. It is therefore necessary to carefully control the operation which, in abrasive blasting applications, would be difficult to achieve without complicating the system design.

Some nozzle designs can be found for cold spray, where a nozzle consists of the converging section fabricated from tungsten carbide or hardened tool steel and the diverging section made of a proprietary non-fouling material [3]. However, the conditions of nozzles in thermal spraying and thermo-abrasive blasting differ since the nozzle in thermal spraying needs to maintain a certain temperature in order to prevent solidification of molten particles and the uniformity of heat transfer is important in the coating processes. Also, the abrasive nozzle is subjected to much higher wear due to the abrasiveness of the blasting media. Although the flame temperature in HVAF is lower than in HVOF processes, it is still considerably high for typical abrasive blasting nozzle materials as shown in Fig. 1.

Fig. 1. The conventional WC-Co blasting nozzle used in thermo-abrasive blasting with signs of material deterioration due to the excessive heat.

Direct measurements of thermal stresses in thermo-abrasive blasting nozzles are difficult to achieve due to high temperatures and a danger of nozzle disintegration. In order to obtain the temperature fields inside the nozzles, the HVAF process was modelled with Computation Fluid Dynamics (CFD) using STAR-CD® software [4]. The simulated temperature field inside the blasting nozzle was applied in the Finite Element Analysis (FEA) of different nozzle materials in order to evaluate the thermal stresses and predict possible failures. The thermal loading of ascending and descending (quenching) types corresponding to the start-up and shut-down cycles were simulated. The nozzles were tested and the temperature of the outer nozzle surface was recorded and compared with the results of the simulation. Some useful properties of the tested nozzles materials are presented in Table 1. Figure 2 shows the WC-Co nozzle arrangement with forced cooling of the nozzle outer surface with compressed air.

Table 1: Nozzle material properties.

Material	Young' s Modulus (GPa)	Poisson's ratio	Tensile Strength (MPa)	Max. Working Temperature (˚C)	Thermal Conductivity (W/m ˚C)	Thermal Expansion (10^{-6}/ ˚C)	Specific Heat (J/kg ˚C)
WC-6wt.% Co	600	0.23	1400	1000	60	5.5	400
SiALON	288	0.23	450	1200	20	3.2	280
SiC	410	0.15	400	1400	25	6	800

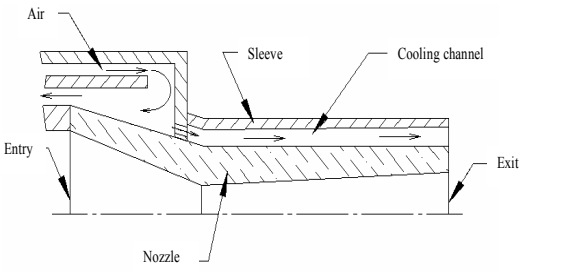

Fig. 2. Section of the WC-Co nozzle arrangement with forced convection on the outer surface.

Figure 3 shows the CFD model of the thermal gun with the nozzle and the cooling layer. The HVAF gun of interest is air-cooled. Subsequently, the flow on top of the nozzle was given as either the buoyancy flow characteristics for free convection or a certain velocity for forced convection.

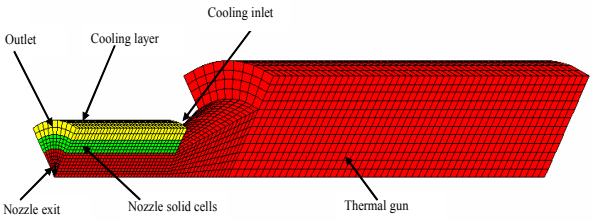

Fig. 3. Computational grid of the thermal gun with the nozzle in the conjugate heat transfer analysis.

Using a conjugate heat transfer analysis, the temperature distribution in the nozzle wall for the different nozzle materials and convection conditions were obtained. For example, Fig. 4 shows the temperature distribution in the WC-Co nozzle with forced convection indicating the temperature difference between the inner and outer surfaces of approximately 300º C.

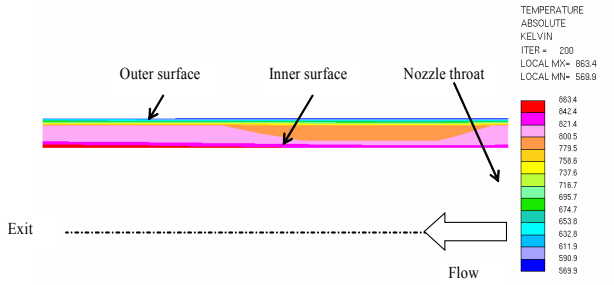

Fig. 4. Simulated temperature distribution in the WC-Co nozzle with forced convection using CFD.

The nozzle inner surface temperatures obtained were used in the transient heat transfer analysis. The outer surface temperatures were compared with the FEA results and the measured values obtained from the experiments.

2. Finite Element Analysis

The heat transfer and the stress analyses were carried out using the FEA software, ALGOR® [5]. Firstly, a transient heat transfer analysis was performed in order to determine the temperature distribution through the nozzle, with the nozzle inner surface temperatures obtained from the CFD analysis. Secondly, a thermal stress analysis was done in order to determine the thermal stress due to the temperature and other factors, such as the applied pressure, the boundary constraints etc.

2.1. Heat Transfer Analysis

Blasting nozzles are symmetrical about their central axis, therefore, a two-dimensional axisymmetrical model with the element thickness of one radian in the hoop direction was used in this analysis. Only one degree-of-freedom is defined for the nodes, the temperature, which corresponds to the Y translation

in elasticity problems. Although there is a swirling flow in the nozzle, the CFD simulation results indicate that there is only a small variation in the temperature distribution in the nozzle inner surface in the circumferential direction.

The initial mesh was refined and a grid-sensitive study was done until consistent results were achieved. The final meshing elements included rectangular and parallelogram elements shown in Fig. 5. The inner surface of the nozzle models was subdivided into a number of patches according to the temperature distribution varying from 300°C to 650°C. The outer surface of the nozzle model was also subdivided into a number of patches in order to apply different convection coefficients to each part of the nozzle model to represent the real cooling conditions. The material model was set to an isotropic type with the conductivity and specific heat independent of temperature as no reliable data for the materials was available.

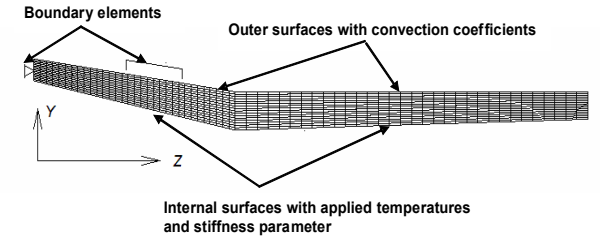

Fig. 5. FE Model of the nozzle.

A heat transfer analysis requires convection coefficients, which are derived from the flow characteristics. In forced convection, the cooling channel was regarded as a duct and a convection coefficient was calculated as follows [6]:

$$h = \frac{Nuk}{D} \tag{1}$$

Where h is the convection coefficient, Nu is the Nusselt number, k is the thermal conductivity of the fluid (air) and D is the duct cross-sectional height.

The Nusselt number for forced convection was calculated using [6]

$$Nu = 0.023\,\mathrm{Re}^{0.8}\,\mathrm{Pr}^{1/3} \tag{2}$$

Where *Pr is* the Prandtl number, *Re* is the Reynolds number, which was obtained from the following [6]

$$\mathrm{Re} = \frac{UD}{\mu} \tag{3}$$

Where U is the flow velocity and μ is the kinematic viscosity.

A convection coefficient for free convection was calculated using the Nusselt number given by [6]

$$Nu = 0.48 \cdot Ra^{0.25} \tag{4}$$

Where *Ra* is the Rayleigh number, obtained from [6]

$$Ra = \frac{g \cdot \frac{1}{(T_w + T_\infty)/2} \cdot (T_w - T_\infty) \cdot D^3}{\mu^2}\,\mathrm{Pr} \tag{5}$$

Where g is the gravity acceleration constant, $\cdot T_w$ is the wall temperature and T_∞ is the fluid temperature.

The convection coefficients for the outer nozzle surfaces were calculated as 1300 and 14 W/m °C for forced and free convection respectively.

For the transient heat transfer analysis of the nozzle models in heating, the temperature load curve for the nozzle inner surface was defined by means of a linear graph assuming that the temperature would rise from 20°C to the values determined in the CFD analysis within the 2 minute-time interval, which was also verified experimentally. Therefore, the temperatures of individual nodes in the boundary layer were controlled as a function of time by using applied temperatures and the thermal stiffness parameter, which is basically a conduction of the thermal boundary element. In comparison, the heat flux in the nozzle inner surface from the CFD analysis was also applied, which produced results deviating by approximately 2%.

Two cases of thermal loading of nozzles in cooling can occur. One is when the thermal gun is switched off and the nozzle cools naturally on the inside since there is no flow of air while the outer surface is forced cooled. This is difficult to model as heat flux distribution from the thermal gun components must be taken into account. In the second case, cooling occurs when combustion is interrupted due to flameout and cold compressed air quenches the nozzle inner surface. Both cases can be considered as thermal shocks.

In modelling for cooling, the initial nodal temperatures were set as the last step of the output file of the transient heat transfer analysis for heating. The convention coefficient of 2800 W/m °C was applied to the nozzle inner surface, which was derived using Eq. (1) with the flow characteristics obtained in the CFD analysis. These include the maximum velocity of 700 m/s and the pressure variation along the nozzle length of 0.5–0.2 MPa. In modelling the normal shut off conditions, free convection was applied to the nozzle inner surface.

2.2. Thermal Stress Analysis

After running the transient heat transfer analysis, the output files for each time interval were used to conduct a static stress analysis with a linear material model analysis. The stress models of the nozzles have

some differences from the heat transfer analysis, such as pressure and boundary conditions, which were added to the initial models. The boundary conditions of the nozzles vary because of the geometry and a method of clamping the nozzles in the thermal gun. Typically, nozzles are clamped in such a way that it allows for thermal expansion. In this case, the *boundary elements* were applied instead of *boundary constraints*, which are elements that are used to connect the finite element model to fixed points in space allowing for some degree of flexibility, which is set by the stiffness parameter.

In order to determine the failure mechanism of nozzle materials, the failure theories were chosen depending on whether the material is classified as ductile or brittle. WC-Co was considered as ductile material and the distortion-energy was applied comparing the Von Mises stress with the yield stress of the material. Ceramics were considered as brittle materials and the maximum-normal-stress theory was applied indicating that the failure occurs whenever one of the three principal stresses exceeds the tensile strength.

In ceramics, the failure can occur due to a crack formation even below the tensile strength characterised by the shock resistance criteria [7]. The shock resistance criteria R_1 and R_2 are applied for severe and mild thermal shocks respectively. The severe thermal shock criterion R_1 corresponds to the maximum allowable temperature difference in a body under conditions of steady-heat flow. The mild thermal shock criterion R_2 corresponds to the maximum allowable heat flux through a body. The shock resistance criteria are determined as following [7]:

$$R_1 = \frac{\sigma (1 - \nu)}{E\alpha} \tag{6}$$

$$R_2 = k \cdot \frac{\sigma (1 - \nu)}{E\alpha} = kR_1 \tag{7}$$

Where E is Young's modulus, ν is Poisson's ratio, α is the thermal expansion coefficient and σ is the thermal stress and is determined by:

$$\sigma = \frac{E\alpha \Delta T}{1 - \nu} \tag{8}$$

Where ΔT is the temperature gradient.

The thermal stresses obtained from the FEA and the shock resistance criteria were used to evaluate the nozzle materials.

3. Simulation Results

The data obtained in the FEA analysis includes the temperature and thermal stress fields in the nozzles at certain time intervals as shown in Figs. 6a and 6b respectively.

The summary of the FEA results is presented as graphs, Figs. 7 and 8.

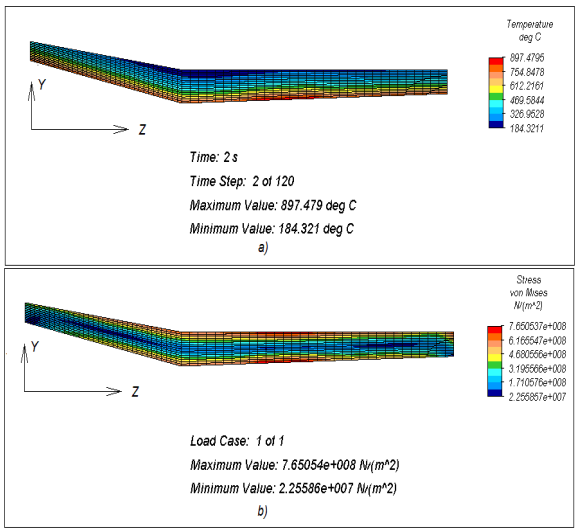

Fig. 6. The temperatures and thermal stresses in the WC-Co nozzle model during rapid heating.

In the case of the WC-Co nozzles, the maximumVon Mises stress of 1000 MPa was obtained, which is below the tensile strength of 1600 MPa indicating that WC-Co nozzles should withstand the thermal shock under present conditions. The maximum Von Mises stress concentrates on the nozzle inner surface.

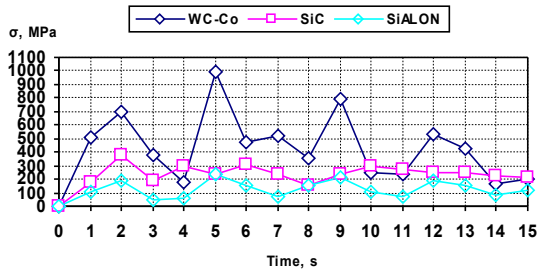

Fig. 7. Maximum thermal stresses in the nozzle materials in rapid heating.

In the case of the SiC nozzle, the highest principal stress of 380 MPa occurred with forced convection and is close to the failure level, Fig. 7. This also corresponds with the thermal shock criteria, which have values just below the maximum thermal shock criteria, Table 2.

For the SiALON nozzles, the highest principal stress of 235 MPa was obtained also with forced convection, which is below the tensile strength of SiALON, Fig. 7.

However, the thermal shock criteria indicate that the SiALON nozzle would not withstand the thermal shock under present conditions, Table 2.

Referring to Fig. 8, in rapid cooling, i.e. flameout, the thermal stresses are lower than in rapid heating but still high in the first three seconds.

Table 2: The calculated shock resistance criteria for the ceramic nozzle materials.

Material	Criterion	Heating	Cooling	Maximum Allowed
SiALON	R_1	196	90	92
	R_2	3927	1800	2763
SiC	R_1	197	142	213
	R_2	20 10^3	14.2 10^3	21.2 10^3

The thermal stresses follow the same trend except for SiALON, which is attributed to the low thermal conductivity of SiALON. The thermal stresses in SiC appear to be the highest among all the materials, which could be attributed to the thickness of the nozzle walls being 10 mm due to manufacturing constraints.

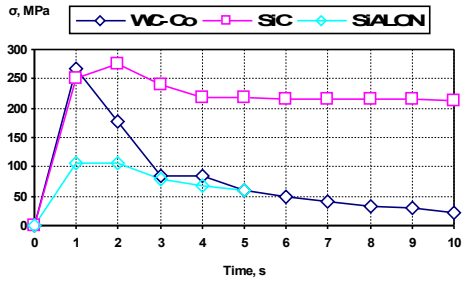

Fig. 8. Maximum thermal stresses in the nozzle materials in rapid cooling.

The thermal stresses are mainly due to the temperature gradient in the nozzle material since no rigid constraints were used in modelling.

4. Experimental Results

The nozzles were tested during start-ups and shut-downs for various cooling conditions. The SiC nozzle withstood the thermal loading during start-up of the thermal gun but failed during rapid cooling, which correlates with the results of analysis with regard to the shock resistance criteria.

Most of the SiALON nozzles failed thermal loading on start-up of the thermal gun, and in some cases in cooling conditions. It was observed that SiALON could withstand thermal loading to a certain degree, for example, with the low fuel/air ratio of 0.01. However, with the fuel/air ratio of 0.02, the SiALON nozzles failed in the area of the nozzle throat as was predicted by the FEA.

The WC-Co nozzle with the 70 mm diverging section withstood the thermal loading and therefore the outer surface temperature could be measured with a thermocouple with the recording time interval of 1 second. In Fig. 9, at approximately 20 seconds from the start of the thermal gun the temperature of the outer surface reached 95°C followed by a period of stability for about 60 seconds. Following this, the temperature increased to 240°C in 35 seconds and finally stabilised. The total time from the start of the thermal gun was approximately 115 seconds. It can be seen that the final simulated and measured temperatures differ by 12%, possibly due to the actual material properties. Also, the FEA results show an exponential increase in the temperature, while in reality there is a period of approximately of 1 min where the outer temperature does not increase, which can be attributed to the thermal properties of WC-Co that change with temperature.

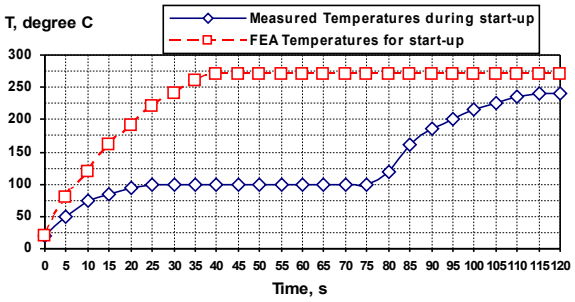

Fig. 9. The measured temperatures of the outer surface of the WC-Co nozzle during start-up of the thermal gun.

When the thermal gun was turned off, a wave behaviour of the temperature was observed for both cases of rapid cooling with the relatively cold compressed air and complete shut off of the air flow inside the thermal gun. As indicated in Fig. 10, the measured temperature sharply decreased from 240°C to 130°C within 10 seconds and then increased to 220°C for 30 seconds, which can be attributed to the heat flux from the thermal gun components, such as the combustion chamber housing and the nozzle holder. This is also believed to be a major contributing factor in ceramic nozzle failures as the heat flux is applied to a relatively small area of the nozzle creating local sites of heat concentration. In comparison, the FEA results follow similar trend for the first 20 seconds, but the rise in the temperatures after 20 seconds was not obtained in the simulation because the heat flux from the components was not included in the modelling.

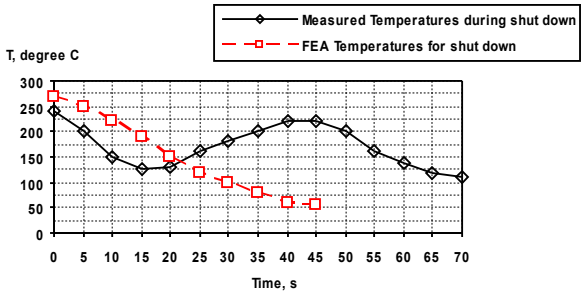

Fig. 10. The measured temperatures of the outer surface of the WC-Co nozzle during shut down of the thermal gun

During trials, the WC-Co nozzles with a 150 mm long diverging section without cooling showed signs of deterioration due to excessive heat as it is believed that a shock wave occurs in the region of 100 mm from the nozzle throat. The flaking off WC-Co could be explained by oxidation of the cobalt in the atmosphere. If the WC-Co nozzles were force cooled, there was no visible material deterioration.

5. Summary and Conclusions

In this study, the typical abrasive blasting nozzle materials such as WC-6wt.% Co, hot pressed dense silicon carbide (SiC) and SiALON (Si_3N_4-Al_2O_3-AlN) were evaluated by means of CFD and FEA modelling and experiments in order to determine their suitability for thermo-abrasive blasting.

From modelling of the thermo-abrasive blasting nozzles and the subsequent temperature gradient, the thermal stress fields and the obtained shock resistance criteria, the following conclusions can be drawn:

- The highest thermal stresses occur in the first 5 – 20 seconds of the start-up and 3 – 5 seconds of the shut down mainly due to the temperature gradient.
- The highest thermal stresses first concentrate on the nozzle outer surface, but after 4 - 5 seconds they concentrate on the nozzle inner surface and specifically around the nozzle throat area.
- The maximum stresses in WC-Co nozzles are below the yield stress and in the experiments, the nozzle withstood thermal loading with and without forced cooling. However, the nozzle diverging length should not exceed 80 mm otherwise forced cooling is necessary to prevent nozzle overheating.
- The maximum thermal stresses and/or the calculated shock resistance criteria in the
- ceramic nozzles exceed the tensile strength and/or the maximum shock resistance criteria indicating that they are not suitable for thermo-abrasive blasting at the present conditions. This was confirmed in trials where the ceramic nozzles failed mainly during start-up.
- In the remaining cases, the ceramic nozzles failed during a sudden flameout, which was attributed to a local heat concentration due to heat flux from the thermal gun components.

Reliable material properties are essential for accurate modelling of the nozzle conditions as thermal properties of ceramics and cermets are temperature dependent.

Acknowledgments

The author wishes to acknowledge Sergey Kotov, for his valuable contribution in the experimental investigation.

References

[1] **Browning J**. *Extreme energy method for impacting abrasive particles against a surface to be treated*. US Patent 5,283,985, 1994

[2] **White R**., *Air and Fuel Mixing Chamber for a Tunable Velocity Thermal Spray Gun*. US Patent 5,520,334, 1996

[3] **Blose R.E., Roemer T.J., Nichols R.T., Mayer A.J. and Beatty D.E**. *Automated cold spray system: Description of equipment and performance data*. Proceedings of the International Thermal Spray Conference, CD ed., E. Lugscheider, Ed., May 2-4, 2005 (Basel), Breuerdruck GmbH, Düsseldorf, Germany, 2005, p 58-66

[4] **Gorlach I.A.** *Thermal stress evaluation of thermo-blast jet nozzle materials*. Ph.D. Thesis, North-West University, South Africa, 2004

[5] https://www.algor.com

[6] **Ozisik M.N**. *Heat Transfer. A Basic approach.* McGraw Hill, Singapore, 1985

[7] **Kingery W.D.** *Factors affecting thermal stress resistance of ceramic materials*. J. Am. Ceram. Soc. , 1955, p 3 –15&